Characterizing the Shapes of Galaxy Clusters Using Moments of the Gravitational Lensing Shear

A.E. Schulz[1,2], Joseph Hennawi[2], Martin White[2,3]

[1] *Harvard University*

[2] *University of California, Berkeley*

[3] *Lawrence Berkeley Laboratory*

Abstract

We explore the use of the tangential component of weak lensing shear to characterize the ellipticity of clusters of galaxies. We introduce an ellipticity estimator, and quantify its properties for isolated clusters from ΛCDM N-body simulations. We compare the N-body results to results from smooth analytic models. The expected distribution of the estimator for mock observations is presented, and we show how this distribution is impacted by contaminants such as noise, line of sight projections, and misalignment of the central galaxy used to determine the orientation of the triaxial halo. We examine the radial profile of the estimator and discuss tradeoffs in the observational strategy to determine cluster shape.

Key words: Gravitational Lensing, Galaxy Clusters

1 Introduction

Clusters of galaxies have long been studied in a variety of contexts as probes of the large scale structure in the universe. It is commonly assumed that clusters are (approximately) isothermal spheres in hydrostatic equilibrium, but this is clearly only an idealization. Key to progress in determining accurate masses and testing our models of structure formation and of gravity is an ability to relax these assumptions in a manner guided by observations. In particular it is of some interest to determine the shapes of the dark matter halos hosting clusters of galaxies; information that is in principle obtainable from studies of gravitational lensing.

Cosmological N-body simulations predict that the dark matter in galaxy clusters collapses into prolate triaxial ellipsoids [1,2]. The conventional belief is that since the baryons are a small fraction of the total cluster mass, baryonic physics has a negligible effect on the halo shape out near the virial radius. However one group [3] has presented evidence to the contrary from numerical simulations of cluster formation which include gas cooling and feedback processes. They suggest that particle orbits are circularized by gravitational interaction with the deeper potential wells from baryonic cooling in the cluster's core, leading to an observable change in halo shape even at large radius. If borne out, this result would have strong implications for our ability to accurately model structure formation on Mpc scales. Such a claim could be tested with data on halo shapes from weak lensing.

Several research groups have looked at characterizing the shape of a dark matter halo using the weak lensing shear distortion [4,5,6,7,8,9]. On galactic scales, [8] reported an observation of halo flattening. They find evidence that the dark matter halos are rounder than the luminous material but that they align well with the light distribution. Ref. [9] present results from the SDSS which are consistent with no flattening. Little observational work exists yet on the shapes of more massive halos, which will be our focus.

Employing the weak lensing shear to characterize cluster ellipticity is not without difficulties. The signal strength in the quadrupole moment is roughly 10 times weaker than the mean tangential shear. This reduction in signal to noise implies that to make a significant detection, observations of several clusters will have to be averaged. The quadrupole moment is also more susceptible to observational systematics (such as the Point Spread Function or PSF anisotropy correction) than is the mean shear. The presence of substructure in the cluster impacts the measurement substantially, as does the projection of other objects in the light cone. On the other hand by working on the high-mass end of the mass function we are maximizing the signal from any given object, and by working with clusters we do not need to worry about the number of objects hosted by any given dark matter halo: our halo occupation distribution is unity above our mass threshold.

The goal of this paper is to identify an assayable estimator from a weak lensing shear observation, Q, that will use the azimuthal variation of the tangential shear to quantify the intrinsic shape of galaxy clusters. Using N-body simulations of dark matter only, we predict the expected distribution of Q for 900 mock observations of galaxy clusters, and we compare the mean result to Q for an elliptical NFW profile. We quantify the impact of contaminants on the quality of the observable signal and identify the minimum requirements needed to resolve the recent controversy on cluster shape.

2 Method and analysis

2.1 Simulations and maps

We have used a sample of 30 simulated N-body clusters. Each cluster generates 31 weak lensing convergence maps obtained by projecting through the volume from different observation angles. The redshift of all clusters is $z = 0.411$, the redshift of the source plane is assumed to be $z = 1$, and both are assumed known. The simulations and ray tracing are the same as those used in [10], while the ray tracing technique is described in [11]. The N-body simulations are extracted from a larger simulation generated with a TPM code [12], with a fiducial cosmology of $\Omega_m = 0.3$, $\Omega_\Lambda = 0.7$, $h = 0.7$, $n_s = 1$, and $\sigma_8 = 0.95$. The simulation volume is a cube with sides of length $320\,h^{-1}\,\mathrm{Mpc}$, with periodic boundary conditions. The 1024^3 dark matter particles each have mass $m_p = 2.54 \times 10^9\,h^{-1}\,M_\odot$. The cubic spline softening length is $\epsilon = 3.2\,h^{-1}\,\mathrm{kpc}$. Clusters are located using a FoF algorithm with linking length $b = 0.2$ in units of the mean inter-particle spacing. Clusters are extracted from the simulation volume in sub-volumes of $5\,h^{-1}\,\mathrm{Mpc}$ [13].

Most of the analysis is carried out on the isolated clusters, but in the instances where we investigate the impact of projection effects from other objects in the light cone, we have added randomly selected cutouts of larger convergence maps calculated with the N-body simulations described in [14] to the convergence maps described above. The fiducial cosmology for these simulations is $\Omega_m = 0.3$, $\Omega_\Lambda = 0.7$, $\Omega_b h^2 = 0.02$, $h = 0.7$, $n_s = 1$, and $\sigma_8 = 1$.

The shear maps are generated from the convergence maps using the Kaiser-Squires method, which is non-local and makes use of the Born approximation [15]. In analyzing our simulations we use the reduced shear because it is the observable quantity [16,17] and can differ from the plain shear in regions where κ is not infinitesimal. Since some of our maps contain convergence values of $\kappa > 1$ at small radii, we have been careful to avoid those regions in the weak lensing shear analysis. We have neglected the rotation effect, but caution that in regions where $\kappa \sim 1$, this may become important. The components of the shear are computed from the Fourier transform of the convergence κ via

$$\gamma_1 = \frac{1}{1-\kappa}\mathrm{FT}^{-1}\left[\frac{\mathrm{k}_1^2 - \mathrm{k}_2^2}{\mathrm{k}_1^2 + \mathrm{k}_2^2}\tilde{\kappa}\right], \quad \gamma_2 = \frac{1}{1-\kappa}\mathrm{FT}^{-1}\left[\frac{2\mathrm{k}_1\mathrm{k}_2}{\mathrm{k}_1^2 + \mathrm{k}_2^2}\tilde{\kappa}\right]. \tag{1}$$

where k_i are the components of the Fourier vector conjugate to 2D sky position and a tilde indicates Fourier transform.

We postulate a family of observable estimators that will quantify the azimuthal

variation of the shear distortion due to the intrinsic shape of a cluster of galaxies. We will call the estimator Q, and generically, it can be computed from a shear map by performing the following integral.

$$Q = \int_0^{2\pi} \int_{\text{annulus}} W(\phi) \cdot \gamma_T(r, \phi) \quad dr d\phi \tag{2}$$

Here $\gamma_T(r, \phi)$ is the tangential component of the weak lensing shear, and is related to γ_1 and γ_2 by $\gamma_T(r, \phi) = -\text{Re}\left[(\gamma_1 + i\,\gamma_2)e^{-i2\phi}\right]$. In the integral, the angle ϕ is defined to be the angle measured from the semi-major axis of the cluster. It is assumed that the tangential shear will be observed in some annulus – the results from different annuli can be combined at a later stage if desired. The overall magnitude of Q scales with $\langle\gamma_T\rangle$, which dies off with radius. To remove this gross trend, we will always present Q normalized to Σ_{SIS} [18], the convergence of a singular isothermal sphere with a velocity dispersion of 1000 km/s. This normalization is purely for presentation purposes and being known analytically in advance, keeps the noise properties of Q simpler than if we had divided by $\langle\gamma_T\rangle$, which would have removed the trend more exactly. Though all radii contain information about the shape, the signal to noise properties will be better in some observational annuli than in others. The weight function $W(\phi)$ can in principle be optimized to select the expected angular variation in tangential shear. In the case where this variation is quadrupolar, $W(\phi) = \cos(2\phi)$. Using $W(\phi) = \cos(2\phi)$ is similar in spirit to the approach presented in [7,9], but without the complication of measuring B-mode signal to control PSF systematics.

Using moments of the gravitational lensing shear to characterize the shape as well as the mass of the underlying dark matter distribution requires that the principle axes of the 2D projection be known. For realistic levels of noise in the shear measurement, we find that it is not possible to determine this direction from the data. Fortunately, there exist other indications of the alignment of an elliptical distribution of dark matter, most notably, the orientation of the cluster's central galaxy (the brightest cluster galaxy or BCG) [19]. However, in the analysis of dark matter simulations, we require a method to determine the the orientation of the semi-major axis, as a reference for measuring the angle ϕ in the integral above. The canonical way of finding the orientation is by computing the moment of inertia tensor I_{ab} of the dark matter particles in the cluster (e.g. [20]). The eigenvectors of this tensor are oriented along the semi-major and semi-minor axes of the object, and the square root of the eigenvalues characterize the cluster's extent along each axis. In this paper we adopt a similar technique, but compute the moment of inertia and the resulting effective ellipticity directly on the 2-D projected κ maps.

The simplest option available for calculating I_{ab} in a map containing only one cluster is to calculate I_{ab} assigning equal weight to each pixel in the map. However this procedure is prone to include nearby structures and objects that

are not part of the cluster, and can skew the resulting orientation of the principle axes. A better scheme is to weight the the map with a function that dies off with radius, such as a 2-D Gaussian distribution. A circular Gaussian apodization biases the computed ellipticity toward rounder values, and occasionally inaccurately identifies the principle axes. We therefore developed a prescription to iterate the calculation of I_{ab}, replacing the initial circular Gaussian window with progressively more elliptical 2-D Gaussians.

Since we assume that a real observation will rely on the BCG in the cluster to identify the axis direction, we choose to find the ellipticity and orientation of the innermost $400\,h^{-1}\,\mathrm{kpc}$; we expect the gravitational environment at that scale to be the dominant contribution to the BCG orientation. We first find the fractional decrease in the average κ at an annulus of radius $200\,h^{-1}\,\mathrm{kpc}$ from the κ at the peak of the cluster. We use this fraction to define the characteristic size of each window in the iteration. We begin with a circular 2-D Gaussian window function, and use the eigenvalues and eigenvectors of the computed I_{ab} to define the next elliptical window function in the iteration. The iteration is continued until both the axis ratio and the slope of the axes have converged to a level of 0.1%. To increase stability and speed, we have forced the change in ellipticity to be monotonic; if the ellipticity in an iteration gets rounder, we elect to update only the slope. To benchmark this prescription, we have applied this technique to elliptical NFW profiles, and have accurately recovered both the ellipticity and the slope. For a small number of N-body clusters, a unique solution for slope and ellipticity could not be identified with this technique, usually due to merging objects that are not well characterized by an elliptical shape. These objects are excluded from our analysis.

The convergence maps from two isolated clusters are shown in figure 1. The shear field is plotted over the top, as are the semi-major (bold) and semi-minor axes. The dashed lines are the axis directions after the first iteration and the solid lines are the converged determination of axis directions. Notice that the bold lines tend to point to regions of higher tangential shear. The cluster on the left has a moderately high ellipticity in the 2-D plane and a relatively small amount of substructure in the region within $\sim 400\,h^{-1}\,\mathrm{kpc}$ where the axes are being determined, thus the initial and converged solutions are virtually identical. In contrast the cluster on the right appears fairly round, and has substructure that affects the direction of the principle axes, requiring six times as many iterations to converge as the cluster on the left.

2.2 NFW profiles and isolated N-body clusters

Using the iterator method to set the direction of $\phi = 0$ in the integral of equation 2, we can now compute the value of Q for each cluster in our sample

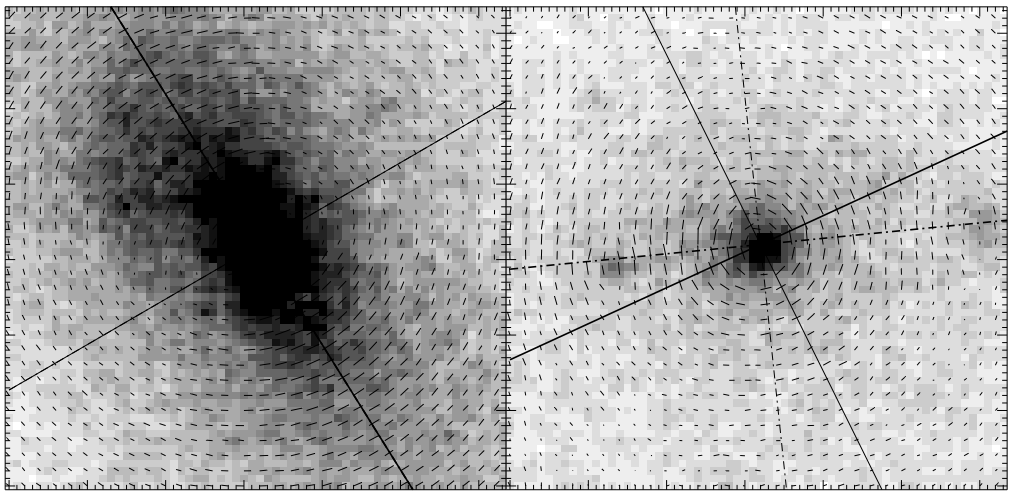

Fig. 1. The κ map, shear field, and principle axes for two isolated N-body clusters. The boxes are 640 h^{-1} kpc on a side. The region affecting the axis determination is somewhat greater than 400 h^{-1} kpc in diameter for more elliptical clusters. The axes plotted are semi-major (bold) and semi-minor axes, where the dashed lines are the initial eigenvectors of I_{ab} and the solid lines are the result after the moment of inertia computation has been iterated to a convergence threshold of %0.1.

using $W(\phi) = \cos(2\phi)$. For our mock observations of Q we select an annulus between $800 - 1000\,h^{-1}$ kpc; large enough to provide an adequate number of background galaxies while not so distant as to lose the signal. We defer justification of this choice to section 2.5. Figure 2 shows Q for each cluster in the sample, as a function of the computed ellipticity. We define ellipticity as $\varepsilon = 1 - b/a$ where b and a are the square roots of the smaller and larger eigenvalues of I_{ab}. Also plotted (solid line) is the value of Q for smooth NFW profiles of the given ellipticity. The NFW profiles used are given by [21]

$$\kappa(x) = \frac{2\kappa_s f(x)}{x^2 - 1} \tag{3}$$

where

$$x = \frac{1}{r_s}\sqrt{x^2(1-\varepsilon) + y^2/(1-\varepsilon)} \tag{4}$$

and

$$f(x) = \begin{cases} 1 - \frac{2}{\sqrt{x^2-1}} \arctan\sqrt{\frac{x-1}{x+1}} & (x > 1) \\ 1 - \frac{2}{\sqrt{1-x^2}} \operatorname{arctanh}\sqrt{\frac{1-x}{1+x}} & (x < 1) \\ 1 & (x = 1) \end{cases} \tag{5}$$

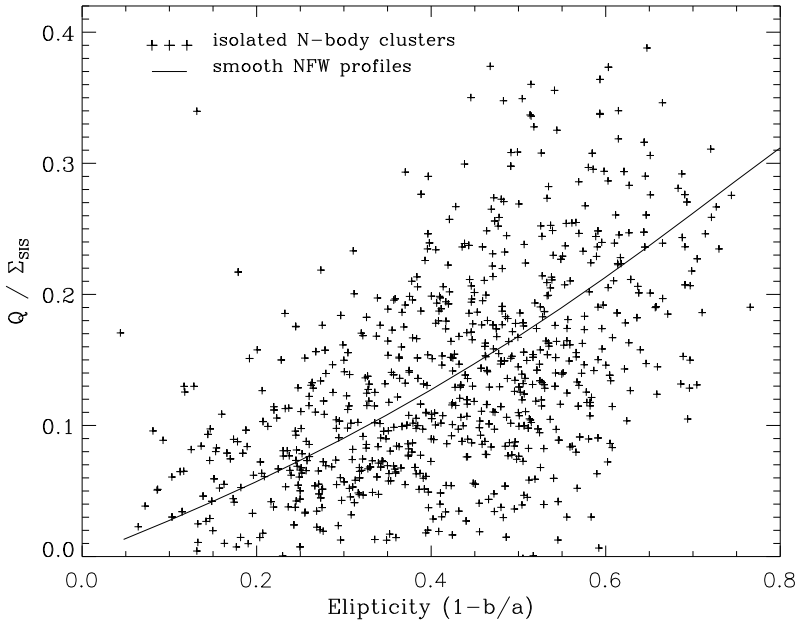

Fig. 2. The computed Q for the N-body clusters in our sample(crosses), as a function of the ellipticity $\varepsilon = 1 - b/a$. We have used $W(\phi) = \cos(2\phi)$. The solid line shows the expected value of Q for smooth NFW profile clusters.

Here $\kappa_s = \rho_s r_s \Sigma_{cr}^{-1}$. Both this parameter and the scale radius r_s are set to their median values for our sample. Values of Q for both the NFW and N-body clusters have been normalized with Σ_{SIS}, the convergence of a singular isothermal sphere at the radius of observation. Figure 2 demonstrates that Q is correlated with ellipticity, but suffers from a large level of intrinsic scatter. This scatter is initially somewhat surprising in light of the fact that the clusters are being studied in isolation, with no projection effects or background noise added into the measurement. The origins of the scatter are threefold; the measurement of Q is extremely sensitive to the existence of substructure in the observed annulus, and is moderately sensitive to how accurately the inner $\sim 400\,h^{-1}\,\mathrm{kpc}$ is aligned with the cluster's orientation at $800 - 1000\,h^{-1}\,\mathrm{kpc}$. The determination of the ellipticity (x axis) is also affected by substructure in the inner $\sim 400\,h^{-1}\,\mathrm{kpc}$ (see right panel of figure 1).

The estimator Q is designed to be sensitive to the azimuthal variation of the tangential shear distortion. This variation can be seen by eye in the right panel of figure 1, wherein the elongation of the shear field vectors is more pronounced near the pointy ends of the cluster. In figure 3, we plot the azimuthal variation of the left cluster in figure 1 (asterisks). This cluster has an ellipticity of $\varepsilon = 0.47$, slightly more elliptical than the mean of our sample ($\varepsilon_{\mathrm{mean}} = 0.414$) and has very little substructure falling into the annulus $800 - 1000\,h^{-1}\,\mathrm{kpc}$. For comparison, we plot the azimuthal profile of a smooth NFW cluster with the same axis ratio (heavy line). To illustrate the effect of substructure in the

observational annulus, we also plot the azimuthal signal of the cluster shown in the bottom panel of figure 3 (wiggly line).

Studying figure 3 yields some insight into the impact of substructure on the observation. In the bottom panel, the 4 circles are at 200, 400, 800 and $1000\,h^{-1}\,\mathrm{kpc}$; the inner two mark the region most impacting the alignment of the BCG and our determination of the ellipticity, and the outer two mark the annulus being observed. Some of the features of this cluster's azimuthal profile are marked with letters. This object differs from the left hand cluster of figure 1 in that it is somewhat more elliptical, thus the amplitude of the tangential shear is larger at point A. Because there is very little substructure in the inner $400\,h^{-1}\,\mathrm{kpc}$, our determination of the principle axes is accurate and the profile is not shifted to the right or left in the top panel. There is substructure at points B, D, E, and F. In the vicinity of these blobs, the shear signal encircles the feature, instead of being tangential to the main part of the cluster. This results in a signal enhancement near the center of the blob, and a suppression to its left and right, where the shear is essentially radial with respect to the cluster center. Substructure causes an effect even when it's outside the annulus, as in D, but the impact is smaller. At point C, the suppression from B and D conspire to create a huge feature in the profile. The substructure at B and E will increase the net Q because $W(\phi)$ is positive in those places. The substructure at points D and F will decrease the net Q. Although it is not shown in this example, substructure in the inner regions can cause the BCG to be misaligned with the bulk of the cluster. This would cause a horizontal shift in the profile plotted in figure 3, and would have the overall effect of decreasing Q in an observed measurement.

2.3 The optimal weight function

In noting the departure of the NFW azimuthal profile from the quadrupolar variation $\cos(2\phi)$ (figure 3), it is interesting to determine whether using a modified shape of the weight function $W(\phi)$ results in a higher quality signal. To this end, we have identified an analytic form that describes the shape of the azimuthal profile for the smooth NFW clusters.

$$F(\alpha,\phi) = \frac{1}{\alpha}\left(e^{\alpha\cos(2\phi)} - 1\right) - P(\alpha) \tag{6}$$

The parameter α monotonically increases with ellipticity. $P(\alpha)$ is an offset that vanishes as $\alpha \to 0$, so that $F(\alpha) \to \cos(2\phi)$ in that limit. The precise dependence of α and $P(\alpha)$ on ellipticity depends on the radius and width of the annulus being observed.

In practice, to test a modified $W(\phi)$, we fit both α and the offset for a sin-

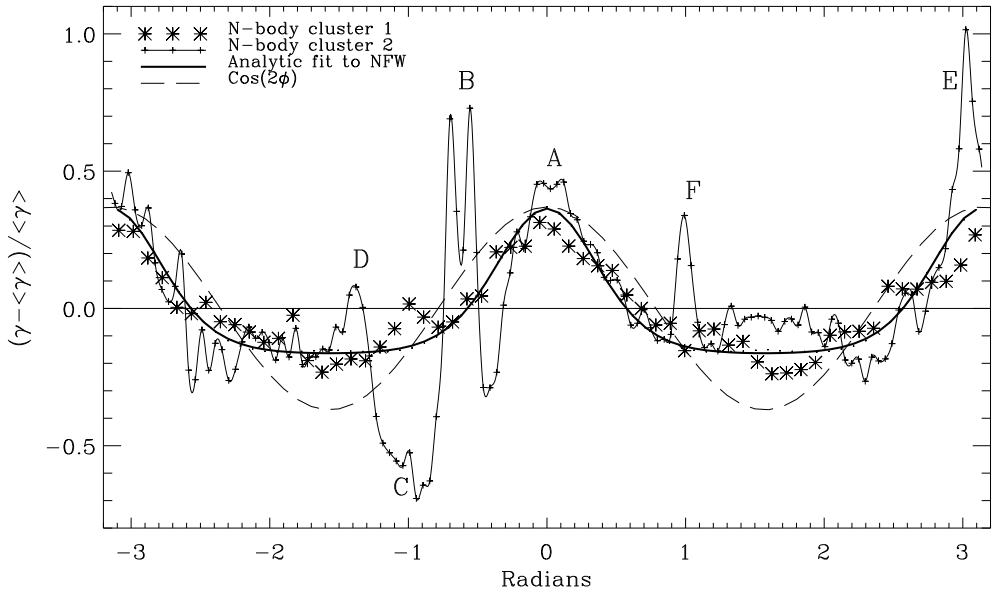

Fig. 3. **TOP** The asterisks show the azimuthal profile of $(\gamma_T(\phi) - \bar{\gamma_T})/\bar{\gamma_T}$ for an isolated N-body cluster. This profile corresponds to the smoother cluster presented in figure 1. The heavy line depicts the azimuthal profile of an NFW cluster with the same ellipticity. The wavy line show the profile of the object below, illustrating the impact of substructure. The labels A-F refer to features in the azimuthal profile, whose angular positions are marked in the figure below. **BOTTOM** This is one of the clusters in our sample that exhibits a high level of substructure in the annulus being observed. The circles have radii $200, 400, 800$ and $1000\,h^{-1}\,\mathrm{kpc}$. The ellipse depicts the axis ratio identified via the moment of inertia in the core.

gle NFW ellipticity, with axis ratio equal to the mean of our cluster sample, $b/a = 0.586$. We used this modified weight function to compute an alternate estimator, Q', and compared it to Q with mixed results. On the one hand, for many of the isolated N-body clusters the strength of the signal is significantly increased, especially for the most elliptical objects. However the intrinsic scatter seen in figure 2 is not improved, and the performance of Q' in the presence of contaminants (see section 2.4) such as instrument noise, projection effects, and misalignment of the BCG is substantially worse than when we use $W(\phi) = \cos(2\phi)$. The peakier profile makes Q' much more sensitive to misalignment of the semi-major axis. Also, since the modified $W(\phi)$ does not integrate to zero, several of the less elliptical clusters with $b/a > 0.586$ wind up with a negative value of Q', which results in a lower mean signal for the sample, and is also difficult to interpret for an individual cluster.

2.4 Noise, projection, and axis misalignment

In practice, a measurement of the quantity Q for real clusters in the universe will be made in the presence of a variety of contaminants. There are a finite number of background galaxies that can be used to measure the shear distortion. They will not be evenly distributed, and the number found will depend on the depth of the observation. Galaxy redshifts will be impacted if they fall close to central BCG or are eclipsed by foreground galaxies. The instrument will also introduce noise in the shear measurement. As is well known, weak lensing measurements suffer from projection effects from objects that lie along the line of sight [22], which in this context is important as these projections have a similar impact on the signal as substructure. Finally, while we have assumed that the BCG will be aligned with the underlying dark matter distribution, in reality its orientation will depend substantially on its merger history, and it has been suggested that under some circumstances, its orientation does not trace that of the larger halo very well [23]. It is important to include these contaminants when predicting an expected distribution of Q observations. In figure 4, we show how projection, noise and misalignment individually impact the expected distribution, and also summarize the result when all three are present. These results are for a sample of $\sim$900 projections through 30 N-body clusters. The histograms are in 26 bins over the domain plotted. The distribution for isolated clusters contains values of $Q < 0$ because of the influence of substructure (see section 2.2).

To model projection, we have added the convergence map of the isolated cluster to a line of sight projected κ map of the same angular size (see section 2.1). Because this method neglects the fact that galaxy clusters often exist in regions of intersecting large scale structure, we expect that we have slightly underestimated the impact of projection effects, but believe our analysis pro-

vides a firm lower bound on the extent of the effect. Objects in the line of sight increase the mean of the distribution by around 7%, and increase the scatter by about 14% in the larger bin. The scatter is affected much less for smaller observational radii, because there is less area in the annulus.

To model the effects of instrument noise and variance in the number of available background galaxies, we have chosen to add a conservative level of white noise to the observation. We postulate that there will be fluctuation per component of the reduced shear of $(\delta\gamma)_{\rm rms} = 0.2$ (where $\gamma_{\rm red} = \gamma/(1-\kappa)$), and that there will be a mean number of background galaxies $\bar{n}_{\rm gal} \sim 100$ per arcminute with which to make a shear measurement. Therefore the noise that we add to each component to get the observed shear is given by

$$\gamma_{\rm obs} = \gamma \pm \sqrt{\frac{(\delta\gamma)^2}{N_{\rm gal}}} \qquad \text{with } N_{\rm gal} = \bar{n}_{\rm gal}\theta^2_{\rm pix} \tag{7}$$

where we ignore intrinsic alignments of the background galaxies, which will be a second order effect. The effect of this noise on the distribution of measured Q values can be seen in the upper right panel of figure 4. The impact is that in the $800 - 1000\,h^{-1}\,$kpc bin the standard deviation is increased by 62% from the inherent scatter. Comparing this to the effects of projection (upper left) and misalignment (lower left), it is clear that this noise is the dominant contribution to the signal contamination, even though achieving a level of $\bar{n}_{\rm gal} \sim 100$ per arcminute will require deep observations from a space based platform.

Perhaps the weakest element in this approach to measuring cluster shape is the reliance on the alignment of the central BCG with the underlying dark matter distribution in the cluster. We have studied the impact of misalignment on the Q values of NFW profile clusters and find that for an NFW profile of mean ellipticity $\varepsilon = 0.414$, a misalignment of 10° leads to a 5% decrease in the measured Q, while a 20° leads to a 30% decrease. In analyzing the N-body simulations, we have tried to be realistic in our determination of the principle axes, in that we have used the inner $\sim 400\,h^{-1}\,$kpc to calculate the expected BCG alignment angle. This means the alignment will be sensitive to the gravitational effects of in-falling substructure near the core. However, since the details of BCG alignment are not known, we have introduced a random scatter in BCG orientation from the eigenvectors of the moment of inertia tensor. The impact of a 15° rms scatter in the BCG orientation on the expected distribution of the observable can be seen in lower left panel of figure 4.

As predicted, introducing misalignment systematically lowers the mean value of Q because the weight function in the integral of equation 2 will have a

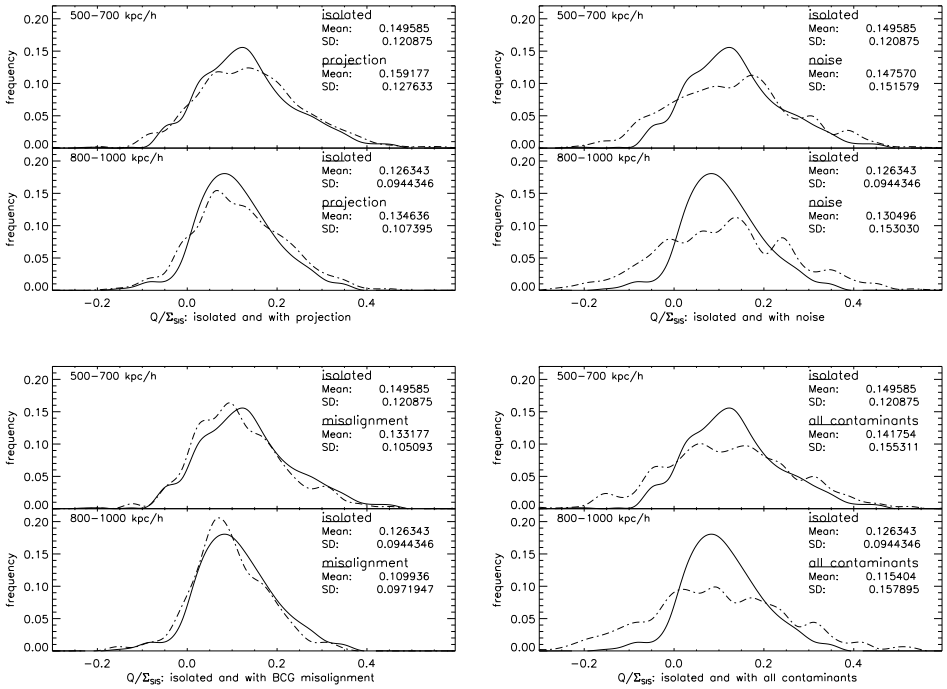

Fig. 4. The histograms demonstrate the impact of contaminants on the expected distribution are shown for two observational annuli. The effects of projection (top left) noise (top right) BCG misalignment (bottom left) are shown separately, and in combination (bottom right). Solid lines mark the distribution without any contamination.

phase lag with respect to the azimuthal variation of the shear. In the $800 - 1000\,h^{-1}\,\mathrm{kpc}$ bin the signal is decreased by around 13%. It is interesting to note that the impact on the spread of the distribution is small. This estimator using $W(\phi) = \cos(2\phi)$ is substantially more robust in the presence of BCG misalignment than one that uses a peakier weight function of the type in equation 6 (denoted Q' above), because $\cos(2\phi)$ provides more overlap with the true signal in the presence of a phase lag. Compare the bold and dashed profiles in figure 3 to see this.

The bottom right panel of figure 4 shows the expected distribution of measured Q values in the presence of all the contaminants. While this distribution is quite broad, it is still a statistically significant signature of the ellipticity of galaxy clusters. The mean ellipticity in our sample of N-body clusters is $\varepsilon_{\mathrm{mean}} = 0.414$, however, connecting the measured value of Q to an effective ellipticity must be done with caution, because substructure causes a large intrinsic scatter in the $Q - \varepsilon$ relationship. Of the contaminants, the most significant is noise in the shear measurement. The standard deviation of Q values is increased by around 67% from the intrinsic level of scatter, and the mean of the distribution is decreased by 9% in the $800 - 1000\,h^{-1}\,\mathrm{kpc}$ bin.

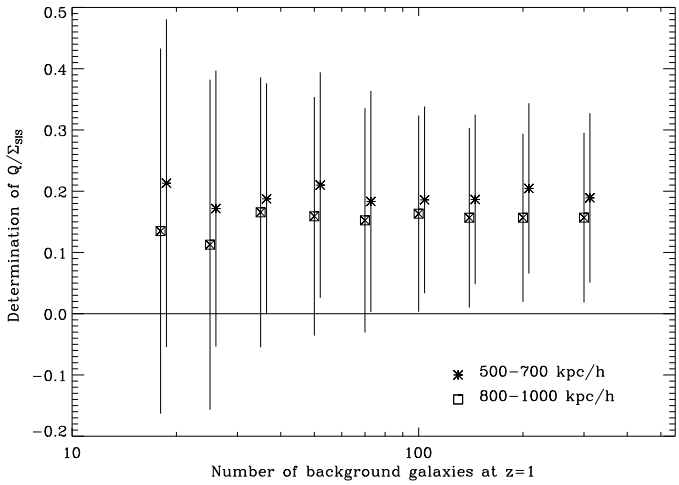

Fig. 5. Mean and scatter of the measured estimator as a function of the number of background galaxies in the observation. Results are shown for annuli at $500 - 700\,h^{-1}\,\mathrm{kpc}$ (asterisks) and $800 - 1000\,h^{-1}\,\mathrm{kpc}$ (squares). Error bars depict 1σ values. Asterisks have been shifted slightly right of the true abscissa for visual clarity.

2.5 Mock observations and noise tradeoffs

Figure 5 shows the results of a mock observation of the estimator as a function of the number of background galaxies. The mean values of Q are plotted along with 1σ error bars indicating the significance of the detection of asphericity on a single measurement. Results are shown for observations performed in two separate annuli, $500 - 700\,h^{-1}\,\mathrm{kpc}$ and $800 - 1000\,h^{-1}\,\mathrm{kpc}$. The abscissa are the same values for each, but we have shifted the asterisks for visual clarity. The plot demonstrates that there are diminishing returns for increasing the depth of the observation to exceed ~ 100 background galaxies per square arcminute. Past this level, the errors are increasingly dominated by projection, BCG misalignment, and intrinsic scatter in the value of Q due to cluster substructure. This scatter cannot be improved by changing the experiment design unless a better method of detecting the orientation of the dark matter halo is discovered. Many ground based experiments that propose to measure the shear distortion will not be able to reach a depth of $100\,\mathrm{arcmin}^{-2}$. Figure 5 implies that in order for these experiments to rule out a spherical dark matter halo using weak lensing shear, they will have to observe closer to the center of the cluster. In practice, this will be difficult to achieve because there will be more confusion in the shear measurement due to foreground galaxies in the cluster.

Figure 6 shows the radial profile of Q/Σ_{SIS} for a sample of around 900 clusters. The solid line shows the radial profile of the the isolated clusters. This result is averaged over the sample; the individual radial profiles exhibit large deviations

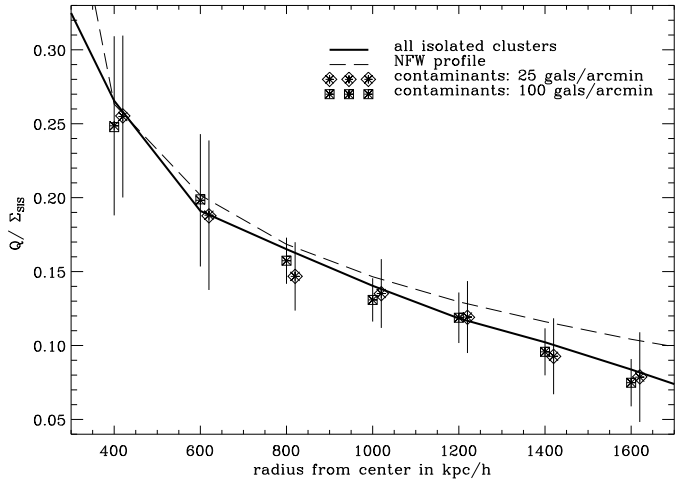

Fig. 6. The radial profile of the estimator Q for isolated N-body clusters (solid), an NFW profile of average ellipticity (dashed), and mock observations of 900 clusters, with contamination from noise, projection effects, and misalignment of the BCG. Noise levels at 100 background galaxies (squares), and 25 background galaxies (diamonds, shifted right). Error bars are bootstrapped 3σ values, and the mock observations are made in non-overlapping annular bins of width 200 h^{-1} kpc.

from this mean. The dashed line indicates the radial profile of a smooth NFW cluster, with the mean ellipticity, and median values for the scale radius and κ_s (see equation 3). The squares indicate the results for a mock observation of about 900 clusters, at a noise level of 100 background galaxies per arcminute, and the diamonds show the result for 25 background galaxies per arcminute. The error bars are bootstrapped from 700 synthetic data sets, each derived from the original data by discarding ~ 330 clusters with replacement. Error bars are plotted at 3σ. The mean values of the mock observation are lower than those of the isolated clusters because random misalignments systematically lower the signal.

Figure 6 suggests that an observation of 900 clusters at 25 background galaxies per arcminute can successfully observe cluster asphericity. It also suggests that with an observation of 900 clusters at a noise level of 100 back ground galaxies per arcminute, it may be possible to distinguish between the predictions of N-body CDM simulations, and those of hydrodynamic simulation in [3], which predict that the ellipticity of dark matter halos is reduced by 20% with the inclusion of baryonic physics. We draw this conclusion loosely, based on the observation that the Q of an NFW cluster of smaller ellipticity $\varepsilon = 0.331$ is reduced by $24 - 25\%$ from the values shown in figure 6. However, we caution the reader that these conclusions are somewhat dependent on our assumptions about BCG misalignment. BCG misalignment systematically reduces the measured value of Q, and is therefore degenerate in its effect with rounder clusters. Another note of caution, we have seen that substructure in

the cluster profoundly affects the measured value of Q. The impact of baryonic physics on substructure is that cooling allows deeper potential wells to form, which may increase the influence of substructure on the measurement. We suggest that changes in the character of substructure may be as important in this type of observation as the changes in the overall shape of the halo. Quantifying this conjecture, however, is beyond the scope of this paper.

3 Conclusions and future work

This work has been a study in identifying an observable estimator of galaxy cluster shape. The estimator, Q, measures the azimuthal variation of tangential weak lensing shear. Using N-body simulations, we have computed the expected mean value and distribution of this quantity. We show that while Q is definitely correlated with ellipticity, there exists a great deal of intrinsic scatter in the relation.

The dominant contribution to the intrinsic scatter is the presence of substructure in the cluster. We have carefully examined the impact of substructure on this estimator of cluster shape. We conclude that substructure at small radii can cause misalignment of the orientation of the innermost region with that of the larger dark matter distribution of the cluster. If this misalignment is reflected in the orientation of the BCG, substructure near the core is expected to decrease the measured value of Q, however, the factors that determine the BCG alignment are not well understood. Substructure in the observed annulus can either increase or decrease the measured value of Q, depending on its azimuthal position with respect to the principle axes. Its effect is to increase the intrinsic level of scatter. It is possible that finding substructure in advance, using a method (e.g. flexion) that is sensitive to small-scale variations in the shear, and then removing it would reduce this source of noise. How well this could be performed on low-S/N data, such as we are likely to have on a per cluster basis, is unclear.

We explored the possibility that the estimator could be improved by matching the azimuthal weight function $W(\phi)$ to the shape of the variation for an NFW cluster of average ellipticity. We find that an estimator of that construction often results in a larger signal for many clusters, but is much less robust in the presence of contaminants, and more difficult to interpret than $\cos(2\phi)$.

There are a few aspects that we have not explored in this work. We have not varied the width of the observational annulus, though our analysis suggests that a wider annulus may be viable (see figure 6). We believe that there is useful information in the radial dependence of Q, and that increased S/N can always be obtained by averaging the noisier results post facto, which

we take as arguments in favor of the narrower annuli we have chosen. We have neglected intrinsic alignments of background galaxies in our treatment of noise, and we have not accounted separately for uncertainties in the redshifts of lenses and sources. We have not sampled large scale structure accurately when including the effects of projection, which has probably caused us to somewhat underestimate the impact. We have relied heavily on the hypothesis that the BCG is somewhat aligned with the dark matter in the galaxy cluster. Finally, we have drawn some loose conclusions about the efficacy of this approach in differentiating the predictions of CDM and the hydrodynamic simulations of [3], but we note that these are likely to be altered by the influence of baryons on substructure. We hope that future work will address these issues.

We have nonetheless made realistic predictions by including the effects of noise, light cone projections, and misalignment of the central galaxy on the distribution of Q. We conclude that the contaminants do not entirely erase the signal, and that a statistical measurement of cluster ellipticity is tractable. We show that even for a reasonably deep observation with 100 background galaxies per square arcminute pixel, observation noise is still the dominant source of uncertainty over the intrinsic level of scatter. We have quantified the relation between the number of background galaxies and the significance of the detection. We have examined the radial profile of Q, and quantified the statistical significance of observations with 25 and 100 background galaxies per arcminute. We conclude that both resolutions should be able to detect cluster asphericity given a sample size of 900 clusters like that analyzed here. The higher resolution measurements that can be made with a next generation space-based platform such as SNAP may be able to distinguish between a mean ellipticity of $\varepsilon = 0.414$ and one that is 20% smaller, enabling us to measure the claimed effects of baryonic physics on cluster ellipticities.

Many thanks to Neal Dalal, Paul Bode, Chris Vale,Masahiro Takada, and Daniel Podolsky for useful discussions about this work. This research was supported in part by grant NSF-AST-0205935, other NSF grants, and NASA. JFH is supported by NASA through Hubble Fellowship grant # 01172.01-A, awarded by the Space Telescope Science Institute, which is operated by the Association of Universities for Research in Astronomy, Inc., for NASA, under contract NAS 5-26555. The simulations were performed on facilities provided by the National Center for Supercomputing Applications (NCSA).

References

[1] J. Dubinski and R. G. Carlberg. *Astrophys. J.*, 378:496, 1991.

[2] M. S. Warren, P. J. Quinn, J. K. Salmon, and W. H. Zurek. *Astrophys. J.*, 399:405, 1992.

[3] S. Kazantzidis, A. V. Kravtsov, A. R. Zentner, B. Allgood, D. Nagai, and B. Moore. *Astrophys. J.*, 611:L73–L76, 2004.

[4] G. Wilson, S. Cole, and C. Frenk. *MNRAS*, 282:501, 1996.

[5] H. Hoekstra, M. Franx, K. Kuijken, and G. Squires. *New Astron. Rev.*, 42:137–140, 1998.

[6] T. G. Brainerd and C. O. Wright. 2000.

[7] P. Natarajan and A. Refregier. 2000.

[8] H. Hoekstra, H. K. C. Yee, and M. D. Gladders. *Astrophys. J.*, 606:67–77, 2004.

[9] R. Mandelbaum, C. M. Hirata, T. Broderick, U. Seljak, and J. Brinkmann. 2005.

[10] N. Dalal, J. F. Hennawi, and P. Bode. *Astrophys. J.*, 622:99–105, 2005.

[11] N. Dalal, G. Holder, and J. F. Hennawi. *Astrophys. J.*, 609:50, 2004.

[12] P. Bode and J. P. Ostriker. *Astrophys. J. Suppl.*, 145:1–14, 2003.

[13] J. F. Hennawi, N. Dalal, P. Bode, and J. P. Ostriker. 2005.

[14] A. E. Schulz and M. White. *Astrophys. J.*, 586:723–730, 2003.

[15] G. Squires and N. Kaiser. *Astrophys. J.*, 473:65, 1996.

[16] P. Schneider, L. van Waerbeke, B. Jain, and G. Kruse. 1997.

[17] M. White. *Astropart. Phys.*, 23:349–354, 2005.

[18] J.A. Peacock. Cambridge University Press, Cambridge, U.K.; New York, U.S.A., 1999.

[19] J. Dubinski. 1997.

[20] J. Bailin and M. Steinmetz. 2004.

[21] M. Bartelmann. *Astron. Astrophys.*, 313:697–702, 1996.

[22] R. de Putter and M. J. White. 2004.

[23] A. H. Gonzalez, A. I. Zabludoff, and D. Zaritsky. *Astrophys. J.*, 618:195–213, 2004.